Physicochem. Probl. Miner. Process., 57(3), 2021, 61-72

http://www.journalssystem.com/ppmp

Physicochemical Problems of Mineral Processing

ISSN 1643-1049

Received February 1, 2021; reviewed; accepted April 4, 2021

Recovery of nickel and iron from low–grade laterite ore and red mud using co–reduction roasting: Industrial-scale test

Xiaoshuang Guo, Chengyan Xu, Yingshuo Wang, Xiaohui Li, Tichang Sun

School of Civil and Resource Engineering, University of Science and Technology Beijing, Beijing, 100083, P.R. China

Corresponding author: chengyan12325@163.com (Chengyan Xu)

Abstract: In this study, the effects of red mud (RM) dosage during the co-reduction roasting of low-grade laterite ore and RM were investigated. The expanded test was conducted under the following optimized conditions: RM-1 dosage of 15 wt%, anthracite dosage of 13 wt%, a roasting temperature of 1300°C, and roasting time of 3 h. Ferronickel powder was obtained with a nickel grade of 1.95 wt%, iron grade of 83.25 wt%, and nickel and total iron recoveries of 94.71 wt% and 95.98 wt%, respectively. The addition of RM improved the recovery of nickel and total iron in ferronickel powder. The reason was because of the increased intensity of the diffraction peaks of kamacite and iron, and the ferronickel particles grown due to the liquid phase were easier to achieve at a lower melting point. The industrial-scale test results showed that ferronickel powder was obtained with average nickel and total iron grades of 1.76 wt% and 86.46 wt%, respectively, which indicated the successful industrial-scale test of co–reduction roasting. Thermodynamic analysis theoretically illustrated the feasibility of the co–reduction of low-grade laterite ore and RM. Increased roasting temperature promoted the reduction of iron oxide and nickel oxide.

Keywords: co-reduction, low-grade laterite ore, red mud, rotary kiln, powdered ferronickel

1. Introduction

The growth of stainless steel and electric vehicle battery production has led to a corresponding increase in the demand for nickel processing (Guo et al., 2018; Li et al., 2019). Low-grade laterite ore, which accounts for approximately 60% of the world's nickel ore reserves, has attracted much attention owing to the dwindling supply of sulphide nickel ore (Tong et al., 2013; Li et al., 2017). However, studies have shown that conventional pyrometallurgical and wet leaching processes are unsuitable for nickel recovery from low-grade nickel ores (Poumaderi et al., 2014; Quast et al., 2015; Sadowski and Pawlowska, 2017; Javanshir et al., 2018). The direct reduction magnetic separation process has proven to be a promising method to recover nickel from low-grade laterite ore (Zhang et al., 2019). The addition of sodium and calcium salts can effectively increase the nickel grade to obtain high-grade ferronickel powder (Jiang et al., 2013; Rao et al., 2013; Wang et al., 2018a). However, the use of additives also causes problems such as increased production costs, the production of a large amount of iron in the tailings that are difficult to use, and the large land area required for their disposal (Lu et al., 2013; Wang et al., 2019). The proper management of these tailings has become an issue with the increasing awareness of the need for environmental protection.

Aluminium is often found in its oxide form, known as bauxite (Liu et al., 2009). Bauxite residue, also known as red mud (RM), is an alkaline waste by-product generated by the extraction of alumina from bauxite (Brunori et al., 2005; Xue et al., 2016a). The global inventory of RM waste has been increasing at an approximate rate of 120 million tons per year (Power et al., 2011). Because of its high alkalinity (pH 10.5-13.0) (Klauber et al., 2011; Panda et al., 2017), the disposal and storage of the vast amounts of RM is a major challenge, which can cause problems such as groundwater contamination, air pollution, and occupation of a large land area (Kirwan et al., 2013; Xue et al., 2016b). However, RM is not considered a

DOI: 10.37190/ppmp/135436

hazardous material in many countries. RM can be recycled as a raw material for the extraction of valuable metals, such as iron, scandium, and aluminium (Yang et al., 2015; Akcil et al., 2018; Gao et al., 2019; Ding et al., 2020). The recovery of other metals is still in the laboratory stage or preliminary exploration stage, except for iron (Zeng et al., 2019). The utilisation of RM in building construction, catalysts, pollution control, and vegetation has also been reported (Taneez and Hurel, 2019; Babisk et al., 2020; Gao et al., 2020; Mishra et al., 2020).

A novel approach called the co-reduction roasting of laterite ore and RM has proven to be feasible in nickel and iron recovery (Wang et al., 2018b). A ferronickel product containing 1.71 wt% nickel and 86.00 wt% iron is produced (Wang et al., 2019), and this technology achieves the effective utilisation of RM by taking advantage of its inherently high alkalinity. However, owing to the equipment and control problems associated with commercialisation, this process remains at the laboratory level (Wang et al., 2020). By collaborating with an enterprise, this paper aimed to validate and promote a practical and efficient co-reduction roasting process to obtain ferronickel products. Expanded tests were conducted to investigate the effects of RM dosage and type on the efficiency of co-reduction roasting and magnetic separation, and determine the optimum roasting conditions. An industrial-scale test was conducted to establish industrial production lines of ferronickel products and achieve an effective and stable operation using an industrial rotary kiln. The roasting temperature and atmosphere in the rotary kiln were controlled in real-time to regularly adjust the operating conditions through online monitoring. To determine the mechanism of the co–reduction roasting process, thermodynamic, X-ray diffraction (XRD), ternary phase diagram, and scanning electron microscope and energy dispersive spectroscopy (SEM-EDS) analyses were carried out. This study provides useful data and bridges the knowledge gap between lab-scale and industrial-scale tests.

2. Materials and methods

2.1. Materials

The low-grade laterite ore used in this study was obtained from Indonesia. The chemical analysis of the sample is presented in Table 1. As seen in Table 1, the nickel grade of the low-grade laterite ore was 0.98%, while the iron grade was 37.57%. The main impurities in the sample were SiO_2, Al_2O_3, and MgO at 11.35%, 12.47%, and 2.57%, respectively. XRD analysis of the low-grade laterite ore in Fig. 1 shows that it mainly exists in the form of goethite (FeO (OH)), lizardite ($Mg_3 Si_2O_5 (OH)_4$), antigorite ($Mg_{3-x}Si_2O_5(OH)_{4-2x}$), quartz ($SiO_2$), and spinel ($Mg (Al, Fe)_2O_4$).

Table 1. Main chemical components of the low-grade laterite ore (wt%)

Component	Ni	TFe*	SiO_2	Al_2O_3	MgO	CaO	Cr_2O_3	MnO	CoO	TiO_2	S
Content	0.98	37.57	11.35	12.47	2.57	2.16	3.92	2.01	0.44	0.34	0.08

Note*: TFe is the content of all iron elements in the corresponding low-grade laterite ore

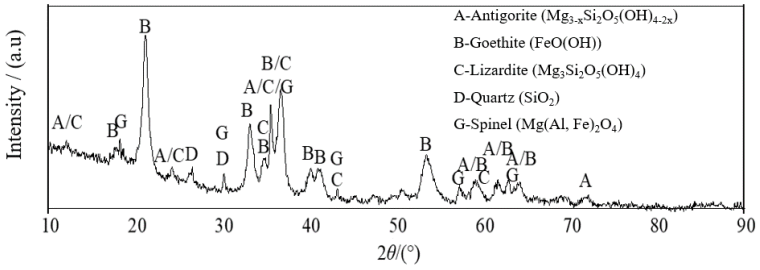

Fig. 1. XRD pattern of the low-grade laterite ore

The RM for the test work originated from GuangXi province, China. In the expanded test, RM-1 was used to study the effects of red mud dosage on the co–reduction process. However, the original RM-1 sample was far from enough on an industrial scale. Therefore, RM-2 was taken from the previous RM-1 location at different batches. Although two different batches of RM were used, their chemical components were not greatly different. The chemical components of the two batches of RM samples are

presented in Table 2. The average values of the different components are also shown in Table 2. The ore samples each contained approximately 27.28 wt% TFe, 15.20 wt% CaO, and 7.03 wt% Na_2O. Besides, RM-1 and RM-2 had similar mineral compositions as shown in Fig. 2. Total iron exists in the form of hematite (Fe_2O_3) and andradite ($Ca_3(Fe_{0.87}Al_{0.13})_2$ $(SiO_4)_{1.65}$ $(OH)_{5.4}$). Sodium is present in the form of cancrinite ($Na_6Ca_2Al_6Si_6O_{24}(CO_3)_2$). Calcium is present as calcite ($CaCO_3$), andradite, and cancrinite.

Anthracite from Shanxi province, China, was used as a reductant and crushed to a diameter of less than 0.5 mm. The industrial analysis of the anthracite based on air-dried materials included fixed 82.38 wt% carbon, 3.48 wt% volatiles, 11.66 wt% ash, 2.48 wt% moisture, and 0.37 wt% total sulphur.

Table 2. Main chemical components of the RM-1 and RM-2 (wt%)

Component	TFe	CaO	Na_2O	SiO_2	Al_2O_3	MgO	S	P
RM-1	24.78	13.94	7.07	10.36	11.94	0.52	0.14	0.1
RM-2	29.78	16.43	6.99	6.99	7.50	0.52	0.14	0.1
Average	27.28	15.20	7.03	8.68	9.72	0.52	0.14	0.1

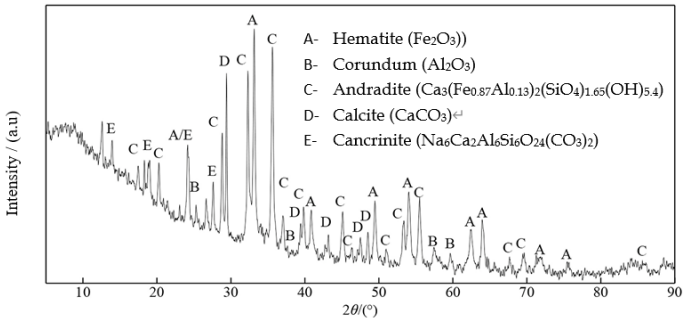

Fig. 2. XRD pattern of RM-1

2.2. Methods

In the expanded test, the mass of low-grade laterite ore was 15 kg. The dosage of anthracite and RM was based on the weight of the laterite ore. These were fully mixed and placed in a SiC crucible, which was subsequently placed in a high-temperature shuttle kiln (JNL-14SA). The anthracite dosage was 13 wt%, the roasting temperature was 1300°C, and the roasting time was 3 h. After each roasting, the co-reduction products were cooled to room temperature, weighed, and crushed to below 4 mm. Then, the co-reduction products were packed under different roasting conditions and sent to the University of Science and Technology Beijing. In the laboratory, the co-reduction products were further crushed to below 2 mm, followed by mixing and splitting. One-stage grinding for 15 min was conducted instead of fine grinding because of the difficulty of achieving the same degree of grinding fineness in each sample (Wang et al., 2019; Wang et al., 2020). The magnetic field strength was 144 kA/m.

The industrial-scale test was performed in an enterprise in Jiangsu province, China. The industrial process flow is shown in Fig. 3. The main processes including raw material mixing, pelleting, rotary kiln co–reduction roasting, grinding, magnetic separation, and product briquetting were described as follows: The low-grade laterite ore was dried through a drying kiln with an inner diameter of 4 m and a length of 32 m, with a moisture content around 10%, then was crushed by a hammer crusher to 100 wt% passing 12 mm. The crushed ore was then mixed with red mud, anthracite, starch, and bentonite for pelleting. Green pellets with a diameter of approximately 50 mm were generated by using a YK1050 pelletizer and then dried in a drying kiln. The prepared green pellets were then put into a rotary kiln (Fig. 4) with an inner diameter of 4.8 m and a length of 70 m for co–reduction. According to the bench-scale test result, the predetermined temperature was kept at 1300°C and the time was 3 h. The heat for the rotary kiln was provided by the liquefied natural gas. After the reduction was completed, the co–reduced pellets were discharged and cooled down to room temperature by water quenching, and subsequently crushed by a jaw crusher and processed by two-stage wet grinding in MQYS3650 grate ball mill (Pulp density in grinding pulp was 60~65% solid by weight.) and MQYS3050 overflow ball mill. CTB-1850 and CTB-1545 magnetic separator was used to separate the ferronickel phase and the

slag. The magnetic product was filtered and then briquetted by an SYST-800 hydraulic molding machine while the non-magnetic product was also was filtered and used for building materials. In the test, 5 wt% bentonite, and 1 wt% starch was added as binders to obtain green pellets.

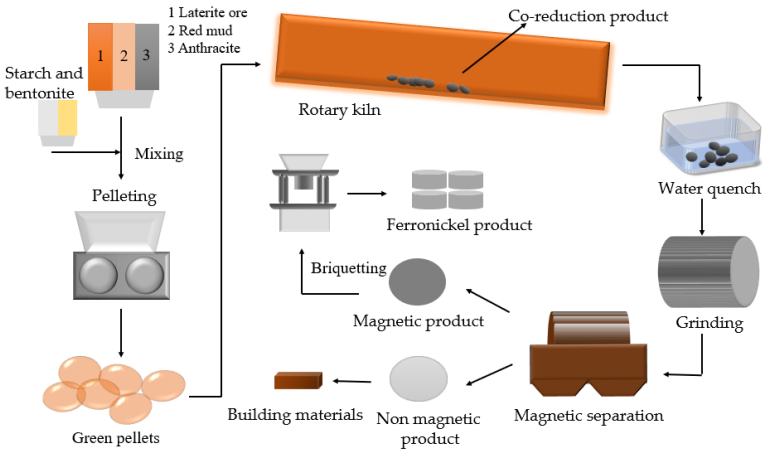

Fig. 3. Sketch of the industrial application of the co-reduction and magnetic separation process

Fig. 4. Overview of the modern industrial-scale rotary kiln in Jiangsu province, China

The grade and recovery of nickel and total iron in the ferronickel product were adopted as the evaluation indices. First, the nickel and total iron grades were analysed by the chemical titration method. The recovery of nickel ε_{Ni} and total iron ε_{TFe} in ferronickel powder was calculated using Eqs. (1) and (2).

$$\varepsilon_{Ni} = \frac{W_F \times \beta_{Ni}}{W_L \times \alpha_{Ni}} \tag{1}$$

$$\varepsilon_{TFe} = \frac{W_F \times \beta_{Fe}}{W_L \times \alpha_{\text{L-Fe}} + W_L \times D_{RM} \times \alpha_{\text{RM-Fe}}} \tag{2}$$

where W_F is the mass of the ferronickel product, β_{Ni} is the nickel grade of the ferronickel product, β_{Fe} is the iron grade of the ferronickel product, W_L is the mass of the laterite ore, α_{Ni} is the nickel grade of the laterite ore, α_{L-Fe} is the iron grade of the laterite ore, D_{RM} is the dosage of RM based on laterite, and α_{RM-Fe} is the iron grade of the RM.

2.3. Analysis and characterization

Mineral compositions were analysed by XRD analysis, which was performed on a Japan Science Ultima IV diffractometer with Cu–Kα radiation (k = 1.5406 Å) in the 2θ range of 10–90° at an operating voltage of 40 kV and a current of 40 mA. The microstructure and particle size were determined using SEM (EVO18, ZEISS, Oberkochen, Germany) equipped with EDS (Quantax, BRUKER, Karlsruhe, Germany).

2.4. Thermodynamic basis for nickel and iron reduction during co–reduction roasting process

Ni, Fe, Cr, and Mn were present in the laterite ore in the form of a corresponding oxide (Table 1). Standard Gibbs energy ($\Delta_rG_m^\theta$) values are shown in Fig. 5, where the dominant reactions of oxides with carbon in the carbothermal reduction system were calculated using HSC Chemistry 7.0.

Fig. 5 shows that the reduction process of iron oxide, in turn, is Fe_2O_3, Fe_3O_4, FeO, and metallic iron. At high temperatures (>1000°C), the reduction of FeO to metallic iron is the dominant reaction. The initial reaction temperature of the carbon gasification reaction is 700°C. The initial reduction temperatures of NiO, FeO, and Cr_2O_3 are approximately 440°C, 710°C, and 1260°C, respectively. NiO and Fe_2O_3 can react with each other and generate $NiFe_2O_4$, which is easily reduced and promotes the reduction reaction. However, in the co-reduction of laterite ore and RM, the $\Delta_rG_m^\theta$ value of this reaction is greater than zero within the experimental temperature range, which indicates that the reaction cannot occur. Therefore, at 1300°C, nickel and iron oxides are easily reduced to metallic nickel and iron, while Cr_2O_3 and MnO are theoretically difficult to reduce to metallic chromium and manganese.

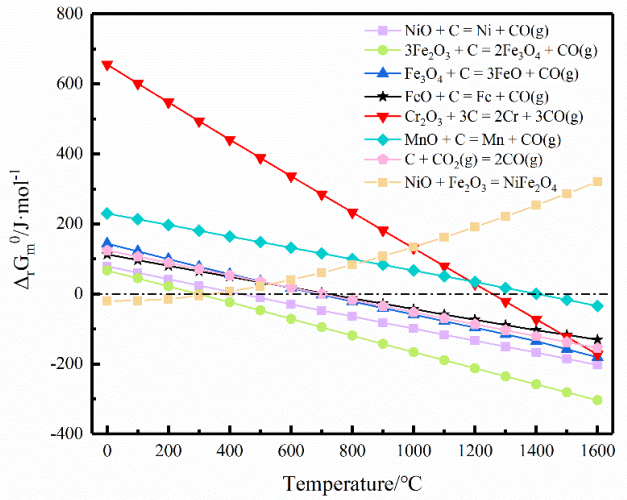

Fig. 5. $\Delta_rG_m^\theta$ of carbothermal reduction reactions during co–reduction process

3. Results and discussion

3.1. Expanded test results

3.1.1. Effects of RM-1 dosages on co-reduction and magnetic separation

The RM type used in the expanded test was consistent with that used in the laboratory. Therefore, the RM dosage test was carried out by using RM-1 with 13 wt% anthracite, a roasting temperature of 1300°C, and a roasting time of 3h to investigate the co-reduction effect in the expanded test. The results are presented in Table 3.

As the RM-1 dosage increased from 0 wt% to 30 wt%, the nickel and iron grade in the raw mixed materials decreased. For the ferronickel powder, the addition of RM-1 increased the iron recovery by at least 10.05 wt%, compared with 0 wt% RM-1. When the RM-1 dosage increased from 0% to 30 wt%, the nickel grade decreased from 2.15 wt% to 1.58 wt%. However, the iron grade changed slightly within the range of 79.31–83.35 wt%. Although the best co-reduction effect was obtained with 10 wt% RM, the RM dosage of 15 wt% was recommended to consume the red mud as much as possible. In the presence of 15 wt% RM-1, a ferronickel powder with nickel and iron grades of 1.95 wt% and 83.25 wt% was obtained, and corresponding nickel and total iron recoveries were 94.71 wt% and 95.98 wt%, respectively. The nickel and total iron recoveries of over 95% indicate that the addition of RM-1 is beneficial to the reduction of low-grade laterite ore.

3.1.2. Effects of RM-1 dosages on mineral transformation

The effects of RM-1 dosage on the mineral compositions of the co-reduction products are shown in Fig. 6. As shown in Fig. 6, the RM-1 dosage showed a significant effect on the mineral transformation of the

co-reduction products. Without RM-1, the main phases of the co-reduction products were olivine and spinel, and small amounts of kamacite and iron. With the addition of RM-1, the intensities of the diffraction peaks of kamacite and iron increased, which indicated that adding RM-1 could promote the co-reduction of laterite ore. This was because RM-1 contained CaO and Na_2O, which strengthened the reduction process and promoted the growth of ferronickel particles. Thus, the recovery of nickel and total iron increased significantly compared with 0 wt% RM-1.

Table 3. Effects of RM-1 dosage on co-reduction and magnetic separation (wt%)

Dosage of RM-1	Mixed materials		Ferronickel powder			
	Iron grade	Nickel grade	Iron grade	Nickel grade	Total iron recovery	Nickel recovery
0	37.57	0.98	79.31	2.15	85.71	89.07
10	36.41	0.89	82.12	2.01	95.76	95.78
15	35.90	0.85	83.25	1.95	95.98	94.71
20	35.44	0.82	82.99	1.80	98.65	92.85
25	35.01	0.78	81.87	1.67	98.87	90.06
30	34.62	0.75	80.43	1.58	98.56	88.92

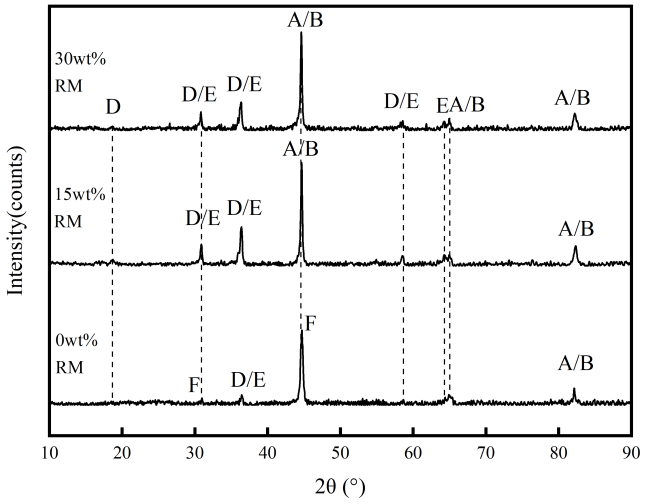

Fig. 6. XRD pattern of the co-reduction products as a function of different RM-1 dosages: A-Kamacite (Ni, Fe); B-Iron (Fe); D- Spinel (Mg (Al, $Fe)_2O_4$); E- Hercynite ($FeO{\cdot}Al_2O_3$); F- Olivine ($(Mg, Fe)_2SiO_4$)

3.1.3. Effects of RM-1 dosages on ternary phase diagram

Melting points were determined by the dosage of the most abundant oxides (CaO, Al_2O_3, and SiO_2) in the material used for slagging (Yu et al., 2013). When the temperature reaches the melting point, a liquid phase is formed and the liquid phase promotes mass transfer and ferronickel particle growth (Li et al., 2015). In this case, examining the melting points of various RM-1 dosages may shed light on the function of adding red mud. For example, the ratio of CaO: Al_2O_3: SiO_2 in the low-grade laterite ore (point A) was 2.57:47.06:50.37. Using FactSage™ 7.3 software, the thermal phase of the CaO-Al_2O_3-SiO_2 system below 1700°C was calculated as shown in Fig. 7. In the absence of the red mud, the melting point was highest, rendering the production of the liquid phase more difficult and requiring a higher temperature. However, the melting point of the system gradually decreased with the addition of RM-1, which indicated that adding red mud in the co-reduction was beneficial to the production of the liquid phase and the growth of ferronickel particles.

In summary, the addition of RM-1 increased the intensity of the diffraction peaks of kamacite and iron, and the liquid phase was easier to produce because of the lower melting point, all of which are beneficial to the growth of ferronickel particles. This is consistent with the results of magnetic separation.

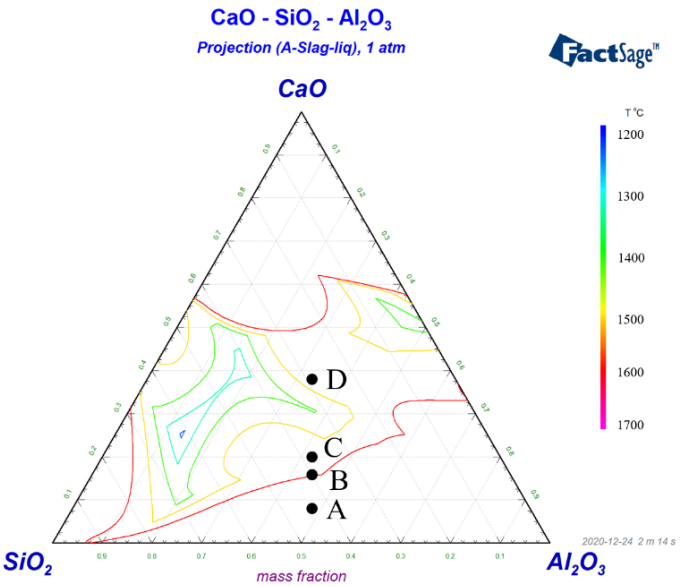

Fig. 7. Ternary phase diagram showing the melting points of various RM-1 dosages in the CaO-SiO_2-Al_2O_3 system below 1600°C. (A) Low-grade laterite ore; (B–C) various dosages of RM-1: (B) 15 wt%, (C) 30 wt%; (D) 100 wt%

3.2. Industrial-scale test results

The effects of RM-2 maintaining an RM dosage of 15 wt% were investigated to determine whether there is any difference in the final indexes of ferronickel powder by adding RM obtained from different batches, and the results are presented in Table 4.

Table 4. Effects of RM-1 and RM-2 on co-reduction and magnetic separation (wt%)

Samples	Mixed materials		Ferronickel powder			
	Iron grade	Nickel grade	Iron grade	Nickel grade	Total iron recovery	Nickel recovery
RM-1	35.90	0.85	83.25	1.95	95.98	94.71
RM-2	36.55	0.85	86.23	1.90	97.13	91.80

Table 4 shows that the addition of RM-1 and RM-2 resulted in iron grades of 83.25 wt% and 86.23 wt%, and nickel grades of 1.95 wt% and 1.90 wt%, respectively. The recovery difference between nickel and total iron was 2.91 wt% and 1.15 wt%, respectively. Overall, the grade and recovery of nickel and total iron in ferronickel powder had little change. RM-2 could be used in industrial-scale tests and a ferronickel powder was obtained with a nickel grade of 1.90 wt%, iron grade of 86.23 wt%, and nickel and total iron recoveries of 91.80 wt% and 97.13 wt%, respectively.

3.2.1. Industrial-scale test under the best roasting conditions

Industrial-scale tests were carried out under the following conditions: 15 wt% RM-2 dosage, 13 wt% anthracite, 5 wt% bentonite, 1 wt% starch, 1300$_o$C roasting temperature, 3 h roasting time, two-stage open-circuit grinding, two-stage continuous magnetic separation, and a magnetic field of 144 kA/m. Continuous operations were conducted from May to September. The production statistics are shown in Table 5 and Fig. 8.

As shown in Table 5, the weight of the monthly total mixed materials gradually decreased from 80739.82 Mg in May to 9012.13 Mg in September; the weight of the corresponding ferronickel powder also decreased each month. However, the yield was relatively stable, ranging from 32.69% to 33.92%. Figure 8 shows that the maximum grade difference between nickel and total iron was 0.12 wt% and 0.52 wt%, respectively. The average grade of nickel and total iron was 1.76 wt% and 86.46 wt%, respectively, which indicated that the quality of the ferronickel powder obtained each month was similar and that the industrial production line maintained uniform stability.

Table 5. Continuous industrial production statistics from May to September

Month	Mixed materials / Mg						Ferronickel powder	
	Wet low-grade laterite ore	Wet-base RM	Anthracite	Bentonite	Starch	Total	Monthly output / Mg	Yield/%
May	58986.20	9092.45	9516.64	2718.39	426.14	80739.82	26984.00	33.42
June	41699.45	6415.37	6709.46	1916.53	300.44	57041.25	19024.37	33.35
July	40976.99	6240.76	6547.94	1870.39	293.21	55929.29	18566.39	33.20
August	35021.57	5240.22	5483.05	1566.21	245.52	47556.58	15546.95	32.69
September	6543.00	1034.86	1078.06	307.94	48.27	9012.13	3056.78	33.92
Total	183227.21	28023.66	29335.14	8379.47	1313.58	250279.06	83178.49	33.23

Note: The yield is the ratio of monthly output of dehydrated ferronickel powder and the corresponding monthly total mixed materials

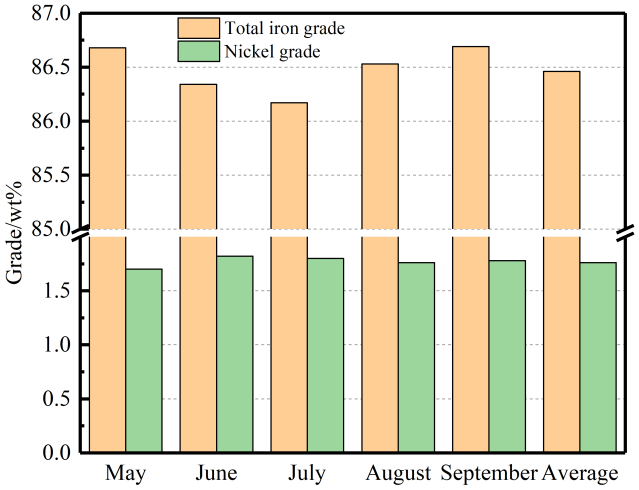

Fig. 8. The grade of nickel and total iron in the ferronickel powder from May to September

3.2.2. Control of the co-reduction roasting using the rotary kiln

In industrial-scale tests, the rotary kiln is the main production plant, while coal ash and temperature reduction are the keys to ring formation. The ringing phenomenon of the rotary kiln is very obvious when the temperature is above 1300°C (Zhang et al., 2020). Therefore, the temperature reduction and atmosphere in a rotary kiln must be controlled in real-time to adjust the operating conditions regularly through online monitoring. The working parts and structure in the rotary kiln are shown in Fig. 9. The key control parameters and the corresponding control measurements are listed in Table 6.

4. Product examination

To determine the success of the above industrial-scale tests in the co-reduction process, multi-element analysis, XRD, and SEM-EDS analyses were carried out.

4.1. Multi-element analysis of ferronickel powder

Samples of ferronickel powder were taken and the quality was evaluated. The results are shown in Table 7.

Ringing is a common phenomenon in rotary kilns. In actual situations, it can be managed as follows: using an anthracite powder with low ash and high ash melting point; maintaining material uniformity; improving pelleting technology and the strength of green pellets, and upgrading the burner.

Table 7 shows that the nickel grade could be raised from 0.98wt% in the raw laterite ore to 1.71wt% in the ferronickel powder and the main impurities in the ferronickel powder were SiO_2 and MgO. Besides, the S content (0.09 wt%) was significantly less than 0.5%, while the P content was slightly below 0.05%.

Nickel grade, iron grade, and other impurities met the required index of steel enterprises. This means that the industrial application of the co-reduction of low-grade laterite ore and RM is successful.

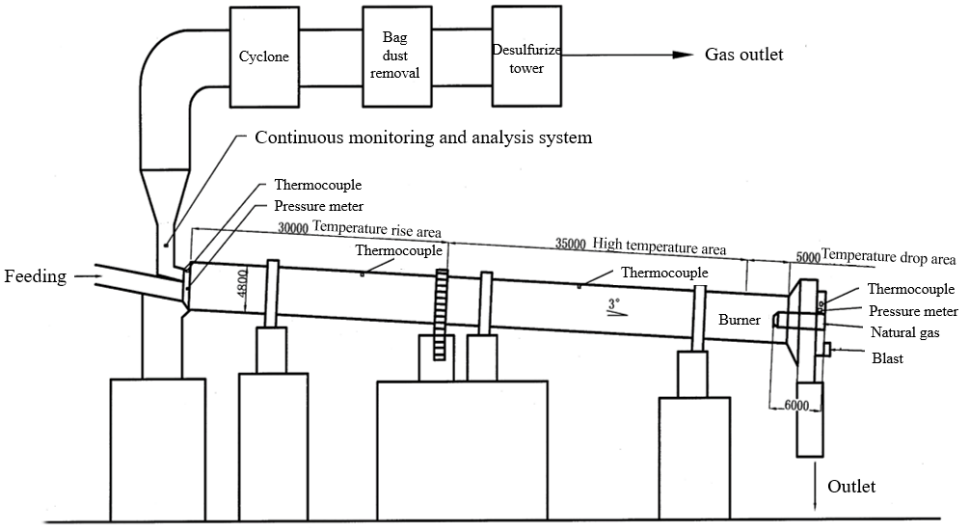

Fig. 9. Sketch of working parts and structure in rotary kiln

Table 6. The key control parameters and the corresponding control measures

Control parameters	Monitoring device	Monitoring location	Monitoring content	Control measures
Temperature control	Handheld infrared thermometer	Kiln head, kiln tail, kiln body, kiln shell, and discharge	Real-time temperature	The discharge temperature at 950-980°C, and the flue gas temperature at 700-750°C
Atmosphere control	A gas continuous monitoring and analysis system; Pressure meter	Kiln head and tail	Real-time gas concentration (CO_2, CO, H_2, CH_4, and O_2)	Ensure reducing atmosphere in the kiln

Table 7. Multi-element analysis of ferronickel powder (wt%)

Component	TFe	Ni	SiO_2	Al_2O_3	MgO	CaO	S	P	C	Cr_2O_3
Required index	>85	>1.6	≤3	-	-	-	≤0.5	≤0.05	≤2	≤0.96
Ferronickel powder	86.76	1.71	2.86	0.90	1.53	0.59	0.09	0.03	0.782	0.87

4.2. Mineral transformation analysis of ferronickel powder

As shown in Fig. 10, the main mineral in the ferronickel powder was kamacite, and the ferronickel powder obtained under the optimum roasting conditions was relatively pure with no other impurities.

4.3. Microstructural analysis of co–reduction product under the optimum roasting conditions

The SEM-EDS of the co-reduction product under 15 wt% RM-2, 13 wt% anthracite, a roasting temperature of 1300°C, and a roasting time of 3 h conditions are shown in Fig. 11.

Fig. 11 shows that nickel and iron mainly existed in the form of kamacite with coarse particles. The main gangue minerals were spinel and olivine. Clear boundaries were observed between ferronickel and gangue particles, which were favourable to subsequent grinding and magnetic separation. It can be seen from Fig. 11(c) that the ferronickel particles obtained under the optimum roasting conditions were relatively pure with no other impurities.

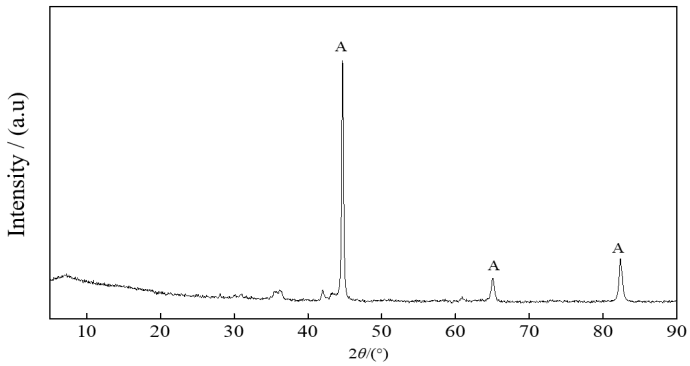

Fig. 10. XRD pattern of ferronickel powder: A-Kamacite (Ni, Fe)

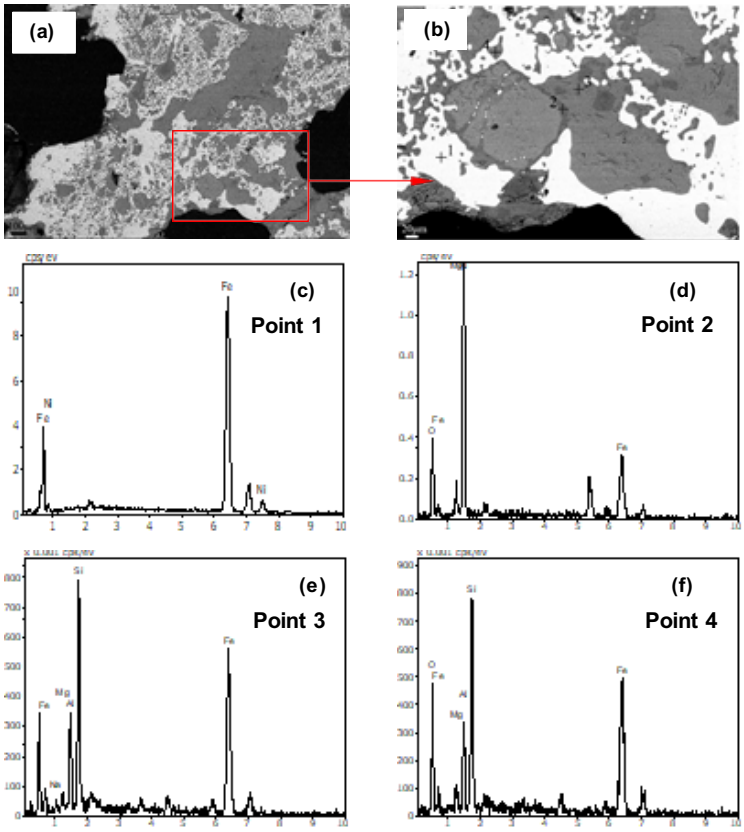

Fig. 11. SEM-EDS of the co-reduction products: (a) SEM image; (b) an enlargement of (a); (c) EDS of Point 1, (d) Point 2, (e) Point 3, and (f) Point 4

5. Conclusions

The followings were obtained from this study:

(1) The optimum conditions for the co-reduction roasting of low-grade laterite nickel ore and RM in the expanded test were as follows: RM-1 dosage of 15 wt%, anthracite dosage of 13 wt%, the roasting temperature of 1300°C, and roasting time of 3 h. Ferronickel powder was obtained with a nickel grade of 1.95 wt%, iron grade of 83.25 wt%, and nickel and total iron recoveries of 94.71 wt% and 95.98 wt%, respectively.

(2) With the addition of RM-1, the intensity of the diffraction peaks of kamacite and iron increased, and the liquid phase was easier to produce because of the lower melting point, all of which are beneficial to the growth of ferronickel particles. This indicates that RM addition can significantly improve the nickel and total iron recoveries from low-grade laterite ore.

(3) In the industrial-scale test, processes of raw material mixing, pelleting, rotary kiln roasting, grinding, magnetic separation, and product briquetting were designed and performed. The production

statistics from May to September showed that the equipment operated properly and the monthly production yield was relatively stable at 33.23%. The average grades of nickel and total iron were 1.76% and 86.46%, respectively.

(4) Thermodynamic analysis theoretically illustrated the feasibility of the co-reduction of low-grade laterite ore and RM. The increased roasting temperature promoted the reduction of iron oxide and nickel oxide. At 1300°C, nickel and iron oxides were easily reduced to metallic nickel and iron, while Cr_2O_3 and MnO were theoretically difficult to reduce to metallic chromium and manganese.

Acknowledgments

This work was financially supported by the National Natural Science Foundation of China (No. 51874017).

References

AKCIL, A., AKHMADIYEVA, N., ABDULVALIYEV, R., ABHILASH, MESHRAM, P., 2018. *Overview on extraction and separation of rare earth elements from red mud: focus on scandium*. Min. Proc. Ext. Met Rev. 39(3), 145-151.

BABISK, M., AMARAL, L., RIBEIRO, L., VIEIRA, C., PRADO, U., Gadioli, M., Oliveira, M., Luz, F., Monteiro, S., Filho, F., 2020. *Evaluation and application of sintered red mud and its incorporated clay ceramics as materials for building construction*. J. Mater. Res. 9(2), 2186-2195.

BRUNORI, C., CREMISINI, C., MASSANISSO, P., PINTO, V., TORRICELLI, L., 2005. *Reuse of a treated red mud bauxite waste: studies on environmental compatibility*. J. Hazard. Mater. 117 (1), 55-63.

DING, W., XIAO, J., PENG, Y., SHEN, S., CHEN, T., ZOU, K., WANG, Z., 2020. *A novel process for extraction of iron from a refractory red mud*. Probl. Miner. Process. 56(6), 125-136.

GAO, C., YANG, G., WANG, D., GONG, Z., ZHANG, X., WANG, B., PENG, Y., LI, J., LU, C., CRITTENDEN, J., 2020. *Modified red mud catalyst for the selective catalytic reduction of nitrogen oxides: Impact mechanism of cerium precursors on surface physicochemical properties*. Chemosphere. 257(C.).

GAO, F., ZHANG, J., DENG, X., WANG, K., HE, C., LI, X., WEI, Y., 2019. *Comprehensive Recovery of Iron and Aluminum from Ordinary Bayer Red Mud by Reductive Sintering–Magnetic Separation–Digesting Process*. JOM. 71(9), 2936-2943.

GUO, Z., PAN, J., ZHU, D., ZHANG, F., 2018. *Co-reduction of Copper Smelting Slag and Nickel Laterite to Prepare Fe-Ni-Cu Alloy for Weathering Steel*. JOM. 70 (2), 150-154.

JAVANSHIR, S., HEIDARI MOFRAD, Z., AZARGOON, A., 2018. *Atmospheric pressure leaching of nickel from a low-grade nickel-bearing ore*. Probl. Miner. Process. 54(3), 890-900.

JIANG, M., SUN, T., LIU, Z., KOU, J., LIU, N., ZHANG, S., 2013. *Mechanism of sodium sulfate in promoting selective reduction of nickel laterite ore during reduction roasting process*. Int J Miner Process.123, 32-38.

KIRWAN, L., HARTSHORN, A., MCMONAGLE, J., FLEMING, L., FUNNELL, D., 2013. *Chemistry of bauxite residue neutralisation and aspects to implementation*. Int J Miner Process. 119, 40-50.

KLAUBER, C., GRAFE, M., POWER, G., 2011. *Bauxite residue issues: II. Options for residue utilization*. Hydrometallurgy. 108 (1), 11-32.

LI, G., LUO, J., PENG, Z., ZHANG, Y, RAO, M., and JIANG, T.,2015. *Effect of quaternary basicity on melting behavior and ferronickel particles growth of saprolitic laterite ores in Krupp–Renn process*, ISIJ Int., 55(9), 1828-1833.

LI, J., CHEN, Z., SHEN, B., XU, Z., ZHANG, Y., 2017. *The extraction of valuable metals and phase transformation and formation mechanism in roasting-water leaching process of laterite with ammonium sulfate*. J. Clean. Prod. 140, 1148-1158.

LI, J., XU, Z., WANG, R., GAO, Y., YANG, Y., 2019. *Study on leaching kinetics of laterite ore using hydrochloric acid*. Physicochem. Probl. Miner. Process. 55(3), 711-720.

LIU, W., YANG, J., XIAO, B., 2009. *Review on treatment and utilization of bauxite residues in China*. Int J Miner Process. 93, 220-231.

LU, J., LIU, S., SHANGGUAN, J., DU, W., PAN, F., YANG, S., 2013. *The effect of sodium sulphate on the hydrogen reduction process of nickel laterite ore*. Miner. Eng. 49, 154-164.

MISHRA, T., SINGH, N., SINGH, N., 2017. *Restoration of red mud deposits by naturally growing vegetation*. Int. J. Phytoremediat. 19(5), 439-445.

PANDA, I., JAIN, S., DAS, S., JAYABALAN, R., 2017. *Characterization of red mud as a structural fill and embankment material using bioremediation*. Int. Biodeter. Biodegr. 119, 368-376.

POUMADERI, S., KESKINKILIF, E., GEVECI, A., TOPKAYA, A.Y., 2014. *Reducibility of nickeliferous limonitic laterite ore from Central Anatolia*. Can. Metall. Quart.. 53 (1), 26-37.

POWER, G., GRAFE, M., KLAUBER, C., 2011. *Bauxite residue issues: I. Current management, disposal and storage practices*. Hydrometallurgy. 108 (1), 33–45.

QUAST, K., OTSUKI, A., FORNASIERO, D., ROBINSON, J.D., ADDAI-MENSAH, J., 2015, *Preconcentration strategies in the processing of nickel laterite ores part3: Flotation testing*. Miner. Eng. 79, 279-286.

RAO, M., LI, G., JIANG, T., LUO, J., ZHANG, Y., FAN, X., 2013. *Carbothermic Reduction of Nickeliferous Laterite Ores for Nickel Pig Iron Production in China: A Review*. JOM. 265 (11), 1573-1583.

SADOWSKI, Z., PAWLOWSKA, A., 2017. *Influence of chemical and biogenic leaching on surface area and particle size of laterite ore*. Physicochem. Probl. Miner. Process. 53(2), 869-877.

TANEEZ, M., HUREL, C., 2019. *A review on the potential uses of red mud as amendment for pollution control in environmental media*. Environ. Sci. Pollut. R. 26(22), 22106-22125.

TONG, L., KLEIN, B., ZANIN, M., QUAST, K., SKINNER, W., ADDAI-MENSAH, J., ROBINSON, D., 2013. *Stirred milling kinetics of siliceous goethitic nickel laterite for selective comminution*. Miner. Eng. 49, 109-115.

WANG, X., SUN, T., CHEN, C., KOU, J., 2018a. *Effects of Na_2SO_4 on iron and nickel reduction in a high-iron and low-nickel laterite ore*. Int. J. Min. Met. Mater. 25 (4), 383-390.

WANG, X., SUN, T., KOU, J., LI, Z., TIAN, Y., 2018b. *Feasibility of co-reduction roasting of a saprolitic laterite ore and waste RM*. J. Int. J. Min. Met. Mater. 25(06), 591-597.

WANG, X., SUN, T., WU, S., CHEN, C., KOU, J., XU, C., 2019. *A novel utilization of Bayer red mud through co-reduction with a limonitic laterite ore to prepare ferronickel*. J. Clean. Prod. 216, 33-41.

WANG, X., SUN, T., WU, S., HU, T., RONG, L., 2020. *Effects and mechanism of Bayer red mud on co-reduction with a saprolitic laterite ore to prepare ferronickel*. Physicochem. Probl. Miner. Process. 56(4), 641-652.

XUE, S., KONG, X., ZHU, F., HARTLEY, W., LI, X., LI, Y., 2016a. *Proposal for management and alkalinity transformation of bauxite residue in China.* Environ. Sci. Pollut. R. 23 (13), 12822-12834.

XUE, S., ZHU, F., KONG, X., WU, C., HUANG, L., HUANG, N., HARTLEY, W., 2016b.*A review of the characterization and revegetation of bauxite residues (RM)*. Environ. Sci. Pollut. R. 23 (2):1120-1132.

YANG, Y., WANG, X., WANG, M., WANG, H., Xian, P., 2015. *Recovery of iron from red mud by selective leach with oxalic acid*. Hydrometallurgy. 157, 239-245.

YU, W., SUN, T., KOU, J., WEI, Y., XU, C., LIU, Z., 2013.*The function of $Ca(OH)_2$ and Na_2CO_3 as additive on the reduction of high-phosphorus oolitic hematite-coal mixed pellets*. ISIJ Int. 53(3), 427-433.

ZENG,H., LYU, F., SUN,W., ZhANG, H., WANG, Y., WANG,Y., 2020. *Progress on the Industrial Applications of Red Mud with a Focus on China*. Minerals. 10 (9), 773-800.

ZHANG, Y., CUI, K., WANG, J., WANG, X., QIE, J., XU, Q., QI, Y., 2020. *Effects of direct reduction process on the microstructure and reduction characteristics of carbon-bearing nickel laterite ore pellets*. Powder Technol. 376, 496-506.

ZHANG, Y., ZHAO, J., MA, X., LI, M., lV, Y., GAO, X., 2019. *Isothermal reduction kinetics and mechanism of pre-oxidized Ilmenite*. Min. Metall. Explor. 36, 825–837.